ACS Catalysis

Research Article

pubs.acs.org/acscatalysis

Enhanced Catalytic Activity of High-Index Faceted Palladium Nanoparticles in Suzuki–Miyaura Coupling Due to Efficient Leaching Mechanism

Gillian Collins,*[,†,‡] Michael Schmidt,[†,‡] Colm O'Dwyer,[†,§] Gerard McGlacken,*[,†] and Justin D. Holmes[†,‡]

[†]Department of Chemistry, the Analytical and Biological Chemistry Research Facility and the Tyndall National Institute, University College Cork, Cork, Ireland

[‡]Centre for Research on Adaptive Nanostructures and Nanodevices, Trinity College, Dublin, Ireland

[§]Materials and Surface Science Institute, University of Limerick, Limerick, Ireland

Supporting Information

ABSTRACT: The structure–property relationship of palladium (Pd) catalysts in Suzuki–Miyaura cross-coupling reactions was investigated using Pd nanocrystals of uniform size and shape. Superior catalytic reactivity was observed for Pd nanoparticles with high-index {730} surface facets compared to low-index {100} facets. Although the nanocrystal morphologies were maintained during the reaction, the presence of Pd clusters, identified by high-resolution transmission electron microscopy (TEM), indicates a leaching mechanism. The nature of the surface facets on the nanoparticles was observed to influence the rate of Pd leaching during the Suzuki coupling reaction. The enhanced reactivity observed for the high-index facet catalysts stems from the greater number of leachable atoms of low abstraction energy available on high-index planes.

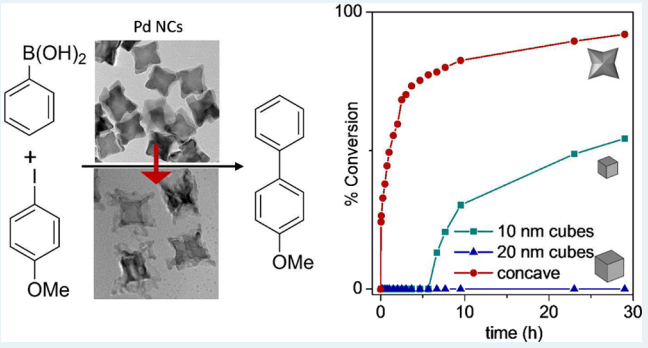

KEYWORDS: *palladium nanocrystals, shape control nanoparticles, Suzuki coupling, leaching*

INTRODUCTION

Noble metal nanocrystals (NCs) with high-index surface facets have attracted much interest due to their potential for enhanced catalytic performance.[1] High index facets are denoted by a set of Miller indices {*hkl*}, where one index is greater than 1. Unlike low-index planes characterized by {111} and {100} facets, which are relatively smooth, the surface atomic structure of high-index facets is characterized by a high-density of step, terrace, and kink sites.[2] Such surfaces are well-known to improve catalytic rates for many reactions.[3] The physical origins of structure sensitivity are complex and generally ascribed to electronic and geometrical effects that influence adsorption energies and reaction pathways.[4] Chemisorption of reaction species can be preferential on step and kink sites due to their lower co-ordination numbers (6–7) or allow more energetically favorable transition states compared to close-packed surfaces.[5]

Pd is an important noble metal as a heterogeneous catalyst for chemical synthesis, automotive, and fuel cell applications.[6,7] Pd is the principle catalyst metal for carbon–carbon cross-coupling reactions, which are central to a variety of chemical processes for pharmaceutical and fine chemicals industries.[8] The versatile nature of these reactions has also led to many other applications such as the surface modification of semiconductors,[9] the preparation of inorganic–organic nanocomposites,[10] and sensors.[11] Coupling reactions conventionally use homogeneous catalysts, but heterogeneous nanoparticle-based catalysts are attractive as they offer convenient removal of the catalyst post reaction. The possibility of recovery and recyclability of the catalyst also makes them more economically attractive, especially for expensive noble metals. A variety of coupling reactions, including Suzuki–Miyaura, Heck, Ullman, Stille and Sonogashira, all proceed under heterogeneous conditions.[6,12−15] Suzuki coupling reactions are one of the most widely utilized methods for the construction of carbon–carbon bonds and are very effective under heterogeneous conditions.[12] Suzuki coupling of aryl chlorides, even deactivated ones, can be achieved under heterogeneous conditions, which are desirable for industrial synthesis due to the low cost of chloride starting materials.[14,16,17]

A wide variety of heterogeneous catalysts have been studied for Suzuki coupling, including dispersed nanoparticles,[18,19] powder-supported nanoparticles,[20−22] and catalytic thin films.[23,24] Several studies have demonstrated considerably enhanced catalytic performance for Suzuki reactions when using NCs enclosed by high-index surface facets.[25−29] A variety

Received: June 10, 2014
Revised: July 23, 2014
Published: July 30, 2014

of preparation methods have been reported for Pd NCs with high-index surface facets such as seeded growth,[27] epitaxial growth,[26,30] and electrochemical[31−33] and solid-state methods.[34] The origin of the enhanced reactivity observed is generally attributed the high density of low-coordinate atoms present at the surface of the catalyst.[2] Early reports of heterogeneously catalyzed Suzuki coupling suggest a surface driven reaction occurring at the edge and corner sites of nanoparticles,[35,36] and this hypothesis is supported by a number of studies providing evidence of a surface-mediated process.[37−39] If a reaction occurs preferentially at edge sites, then enhanced reactivity reported for high-index planes compared to low-index planes would be reasonable because of the stepped nature of high-index facets. A considerable number of mechanistic studies have identified that leaching processes occur in many nanoparticle catalyzed reactions.[40−42] Although debate still surrounds the leaching mechanism, dissolved Pd from the nanoparticle surface has been shown to play a central role in the catalytic cycle of Suzuki reactions.[43,44]

Here, we investigate the structure−property relationship of catalysts in Suzuki cross-coupling reactions using Pd catalysts of uniform size and shapes. The catalytic reactivity of Pd nanoparticles with low-index {100} facets and high-index {730} facets are compared. Considerably improved catalytic performance was observed with high-index facet NCs. Catalytic studies, high-resolution electron microscopy, and XPS analysis were used to elucidate the mechanism of the enhanced reactivity associated with the high-index surface planes. We identify that the superior activity observed for the high-index faceted catalysts stems from the greater leaching of Pd atoms from the surface rather than a true surface-mediated process.

EXPERIMENTAL SECTION

Pd NC Synthesis. Cubic NCs with edge lengths of 10 and 20 nm were synthesized as previously described and used for the seeded growth of the concave NCs.[27] The mean edge length was determined to be 10.6 nm (standard deviation, σ = 1.3) and 19.4 nm (σ = 1.9) for the cubic NC and 35.1 nm (σ = 3.2) for the concave cubic NCs (Supporting Information Figures S1 and S2). These nanoparticles are capped with PVP and Br capping ligands. To avoid the influence of support materials on the catalytic activity of the NCs, unsupported nanoparticles were used.

Materials Characterization. Scanning electron microscopy (SEM) images were obtained using a FEI DualBeam Helios NanoLab 600i high-resolution SEM. Transmission electron microscopy (TEM) analysis was performed using a Jeol 2100 electron microscope at an operating voltage of 200 kV. X-ray photoelectron spectroscopy (XPS) was performed using a KRATOS AXIS 165 monochromatized X-ray photoelectron spectrometer equipped with an Al Kα (hv =1486.6 eV) X-ray source. Spectra were collected at a takeoff angle of 90°, and all spectra were referenced to the C 1s peak at 284.6 eV.

Catalytic Studies. In a typical reaction, 0.268 g of phenylboronic acid (2.2 mmol), 0.468 g of 4-methoxyiodobenzene or 0.25 mL of 4- methoxybromobenezene (2 mmol), and 0.553 g (4 mmol) of K_2CO_3 were added to 30 mL of ethanol/water (3:1). The reactions were initiated by addition of the catalyst. Reactions were conducted at room temperature and sampled at regular intervals for GC analysis. Samples were analyzed using an Agilent 7890A GC system, equipped with a flame ionization detector (FID). Products were identified against authenticated standards and quantified by calibration to obtain response factors (RF) against the known internal standard (dodecane). The turnover number (TON) and turn over frequency (TOF) were calculated on the basis of the amount of biaryl product formed. The TON^{surf} and TOF^{surf} are the TON and TOF normalized to the number of surface Pd atoms. The number of surface atoms on cubic and concave cubic NCs was calculated on the basis of geometrical considerations assuming a face-centered cubic (fcc) Pd lattice. The total number of Pd atoms per NC was estimated by the volume of a cube or concave cube/volume of the unit cell $(3\sqrt{a}) \times$ the number of atoms per unit cell (4), where a is the lattice constant for fcc Pd, taken to be 0.389 nm. The total number of surface atoms was estimated by surface area of the cube/surface area of the two-dimensional lattice × 2. For concave cubes, this relationship was multiplied by 3/7 assuming the atomic density of the {730} surface facets is 3/7 that of the {100} facets. The volume of a concave cube was approximated by taking the volume of a cube minus the volume of the square pyramids occupying the six sides of a cube.

RESULTS AND DISCUSSION

Figure 1a,c show TEM images of cubic NCs enclosed by six {100} surface facets, with close-packed atoms and a surface

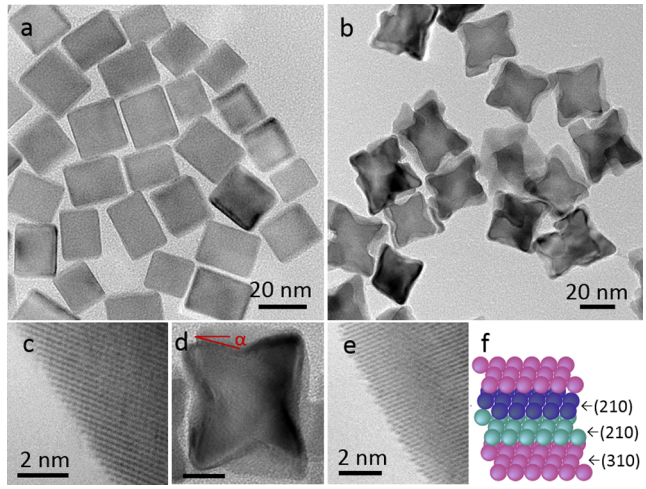

Figure 1. TEM image of as-synthesized (a) 20 nm cubic Pd NCs, (b) concave cubic Pd NCs. (c) Surface of cubic NCs, (d) surface of concave cubes, (e) surface of concave cubic NCs, and (f) schematic illustrating the {730} facet. Scale bar in (d) is 10 nm.

atom co-ordination number of 8. Figure 1b shows a TEM image of concave cubic Pd NCs that measure 20 nm across and 35.1 nm from corner to corner. On the basis of angle projection along the [001] direction,[27] the faces can be indexed to the {730} surface facet, as shown in Figure 1d.[2] A {730} facet consists of a periodic series of two (210) facets and one (310) facet, as illustrated in the TEM in Figure 1e and the schematic in Figure 1f. The density of step surface atoms is ~5 × 10^{14} cm^{-2}, which implies that ~40% of surface atoms are located at step sites. The catalytic performance of the low- and high-index surface planes was compared in the cross-coupling of 4-methoxyiodobenzene (1) acid and phenylboronic acid (2) in $EtOH/H_2O$, as illustrated in Scheme 1.

Figure 2 shows the reaction profiles for cubic (10 and 20 nm) and concave cubic NCs and reveals significant differences in the catalytic behavior with both size and shape effects

dx.doi.org/10.1021/cs5008014 | ACS Catal. 2014, 4, 3105−3111

Scheme 1. Model Suzuki–Miyaura Reaction Used in This Study

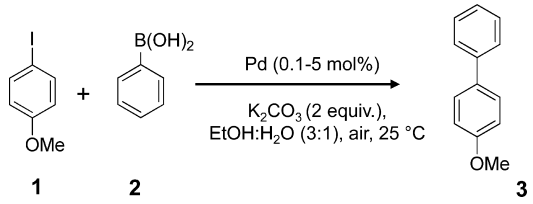

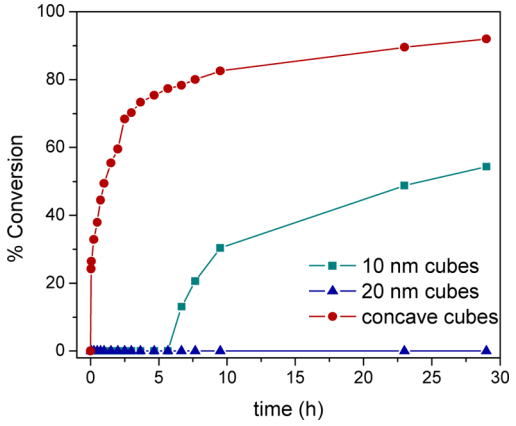

Figure 2. Reaction profile of Suzuki coupling reactions using Pd NCs with high- and low-index facets.

observed in the catalytic activity. The concave cubes and 10 nm cubic catalysts were found to be active for the coupling reaction, whereas the 20 nm cubic NCs showed no reactivity, at a Pd concentration of 0.5 mol %. The enhanced catalytic activity of the high-index surface facets is apparent, with the yield of biphenyl product increasing from 54% for cubic catalysts to 92% for concave cubic catalyst, after 30 h. This reactivity represents more than a 6-fold increase in the TON for the high-index surfaces (TON = 7077) compared to low-index planes (TON = 1073), after normalization to the number of surface atoms for each NC. Both the 10 and 20 nm cubic catalysts were found to be inactive for the coupling of 4-methoxybromobenzene and phenylboronic acid, although concave cubes displayed similar reactivity to the aryl iodides, achieving an 89% yield. No induction period was observed for the concave cubes, whereas the reaction catalyzed by the cubic catalysts displayed a considerable lag time of 300 min, as shown in Figure 2.

Figure 3a,b show SEM images of the cubic and concave cubic catalysts collected after the reaction, respectively. The catalysts showed negligible change to their morphology, and the well-defined surface facets were intact, as shown by the inset TEM images. Although the NCs showed little change to their overall shape, a slight reduction in the mean edge length and a boarding in the size distribution was observed. The mean edge length for the 10 nm cubic NCs decreased from 10.6 nm (σ = 1.3) to 9.6 nm (σ = 1.9), while the edge length for the concave cubic NCs decreased from 35.1 nm (σ = 3.2) to 31.6 nm (σ = 3.9) (Supporting Information Figures S1 and S2). Negligible changes to the edge length of the 20 nm cubic NCs was observed—19.5 nm (σ = 1.9) before and 18.9 nm (σ = 2.1) post reaction. Detailed TEM analysis revealed the presence of small nanoparticles about 1–2 nm in diameter, in the Pd residue collected after the reaction, as shown in Figure 3c,d. High-resolution imaging of these particles, shown in Figure 3c,d

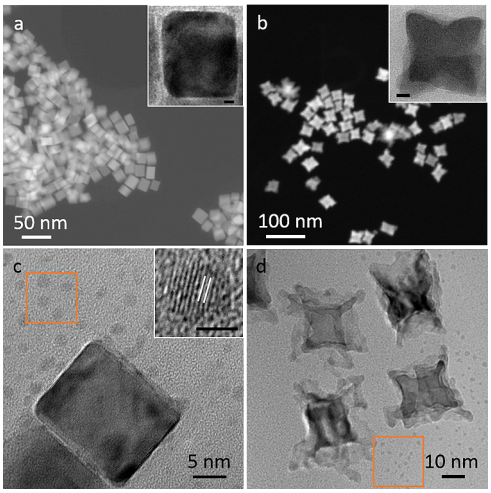

Figure 3. SEM image of cubic Pd NCs and (b) concave cubic Pd NCs cubes after a Suzuki coupling reaction (0.5 mol %). Insets in (a) and (b) show TEM images of the individual NCs. Scale bars in insets are 2 nm. (c) TEM image of cubic NCs and (d) concave NCs Pd 0.1 mol % after the reaction showing dissolution and the presence of small diameter Pd nanoparticles. Scale bar insets of (c) and (d) are 2 nm.

insets, indicates a *d* spacing of 0.23 nm, which can be attributed to Pd(111) lattice fringes.[23] Pd clusters are observed in the TEM grids of both low-index and high-index particles. These particles were not present in the as-synthesized solution of the catalyst NCs and so can be attributed to leached Pd during the reaction.[45] Notably, Pd clusters of 1–2 nm in diameter only comprise ~200–300 atoms, which accounts for about 0.4% of the total atoms in a 10 nm cubic NC. Significant changes to the NC morphology were not readily apparent at high catalyst concentrations (0.5 mol %), consistent with previous reports.[27] When the Pd catalyst concentration is decreased to 0.1 mol %, after reaction at room temperature, dissolution of the concave cubic structures was clearly observed, as shown in Figure 3d. Figure 2 also demonstrates the lower activity of the 20 nm compared to 10 cubic NCs, which fail to catalyze the reaction at a Pd concentration of 0.5 mol %. If the surface of the cubic NCs were solely the active sites, then the surface normalized TONs should be similar for both the 10 and 20 nm cubic NCs, which is not the case. The lower activity of the 20 nm cubic NCs is attributed to the lower leaching susceptibility, which may be correlated to the greater stability of the 20 nm cubic NCs compared to the 10 nm NCs.[46] The superior stability of the larger cubic NCs leads to less leaching and therefore reduced catalytic performance in the coupling reaction.

The effect of catalyst concentration was assessed, and Figure 4 shows the reaction profiles of cubic and concave cubic NCs with a Pd concentration of 0.1, 0.5, 1, and 5 mol %. The TONs and TOFs for the different catalyst concentrations are shown in Table 1. Cubic NCs (Figure 4a) displayed an increased conversion rate with increasing Pd concentration. No conversion was observed with a Pd concentration of 0.1 mol %. Similarly, although the 20 nm cubic NCs (Figure 4b) gave no conversion at 0.5 mol %, yields of 32% and 48% could be achieved with 1 and 5 mol % Pd, respectively. Interestingly, the concave cubic catalysts did not exhibit the same reactivity trend, with varying catalyst concentration. As shown in Figure 4c, a Pd concentration of 1 mol % was faster than a higher catalyst concentration of 5 mol %. Figure 4d shows a magnification of the first 180 min of the reaction, illustrating that initially the 5

dx.doi.org/10.1021/cs5008014 | ACS Catal. 2014, 4, 3105–3111

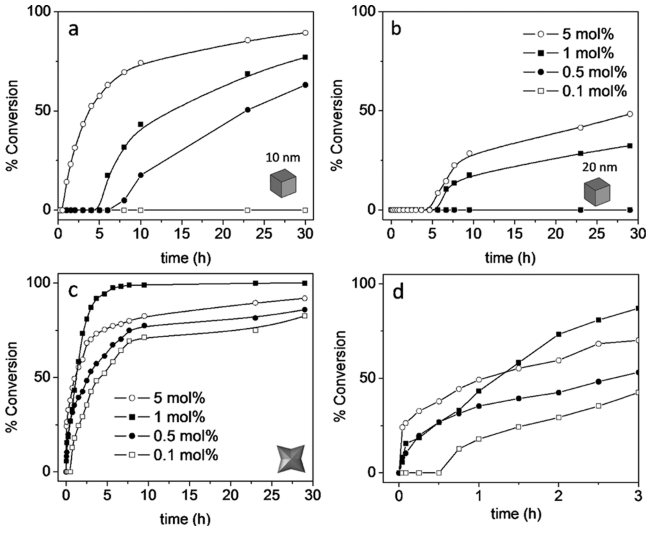

Figure 4. Reaction profile with varying Pd concentrations for (a) 10 nm cubic NCs, (b) 20 nm cubic NCs, and both (c) and (d) concave cubic NCs.

Table 1. Effect of Catalyst Concentration for Cubic and Concave Cubic NCs in Suzuki Coupling[a]

catalyst (mol %)	yield (%)	time (h)	TON^{tot}	TON^{surf}	TOF^{surf}
cube (10 nm)					
0.1	0	30	0	0	0
0.5	59	30	118	1073	38
1	77	30	77	700	23
5	89	30	17.8	161	5
cube (20 nm)					
0.1	0	30	0	0	0
0.5	0	30	0	0	0
1	32	30	32	533	18
5	48	30	9.6	160	5.3
concave cube					
0.1	72	9.5	720	28 000	3032
0.5	89	9.5	178	6846	721
1	100	9.5	100	4000	133
5	83	9.5	16.6	638	67

[a]See Experimental Section for calculation of TOFs.

mol % displayed the fastest conversion, but the reaction slowed as it progressed. This inverse relationship between the Pd concentration and rate has been associated with a homogeneous mechanism.[47] Deactivation of this so-called *homeopathic* Pd occurs as the solubilized Pd nucleates to form Pd clusters that continue to grow.[48,49] Quenching of the catalytically active Pd species in solution becomes more efficient as the Pd concentration increases due to greater leaching.[15] TEM analysis also provided evidence for this deactivation mechanism at higher Pd concentrations, which showed the presence of Pd aggregates compared to discrete nanoparticles observed at lower Pd concentrations (Supporting Information Figure S3). It is worth noting that although leaching is identified as an important step in the catalytic activity of the NCs, it does not identify the nature of the catalytic species (i.e., if the reaction is catalyzed by molecular Pd or the small diameter clusters observed by TEM). The leached Pd species exist as solubilized Pd in equilibrium with the Pd clusters, and it is not possible to distinguish if the catalytically active species is homogeneous or heterogeneous in nature.

A significant difference in the catalytic behavior is the absence of an induction period for the high-index NCs and a very long induction time for the cubic NCs. Lag periods have been attributed to the time required to leach sufficient Pd into solution for catalytic turnover. On the basis of the TEM analysis indicating a homogeneous mechanism, the absence of an induction period for the concave cubic NCs suggests rapid leaching from the NC surfaces. To investigate if the induction time was associated with Pd leaching, the reaction catalyzed by the cubic NCs was stopped after 60 min, by which time no biphenyl product was formed, and the presence of Pd clusters was not observed by TEM analysis. In comparison, when the reaction catalyzed by the concave cubic NCs was stopped after 60 min, when conversion is at 38%, the presence of the leached Pd clusters were observed by TEM (Supporting Information Figure S4). Although TEM cannot quantify the leached Pd, it qualitatively shows that the presence of leached Pd, in the form of molecular or clusters, plays a central role in the catalytic activity.

To further investigate the reaction regents that contribute to leaching, the cubic NCs (0.5 mol %), which have a long induction period, were prestirred separately in solutions of the aryl iodide, boronic acid + K_2CO_3, K_2CO_3, and $EtOH/H_2O$ for 3 h, after which time the remaining reagents were added. The reaction profiles were monitored to determine if the conversion rates improved due to leaching. Figure 5 compares the reaction

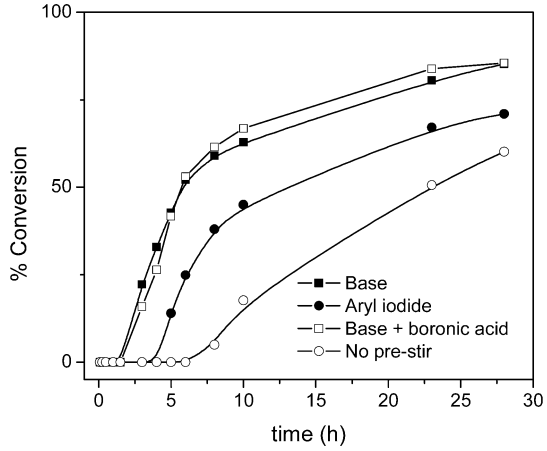

Figure 5. Influence of prestirring cubic catalysts in solutions of K_2CO_3, 4-methoxyiodobenzene, K_2CO_3 + phenylboronic acid. NCs prestirred in $EtOH/H_2O$ showed no difference to the control and are omitted for clarify.

profiles of the prestirred solutions and a control reaction where no prestir was conducted. All of the prestirred solutions except the $EtOH/H_2O$ solvent exhibited faster reactions, with the base and boronic acid having the most influence, increasing the yield from 59% to 90% without the prestir. The faster conversion was observed for the prestir samples suggesting leaching of Pd occurs and that all the agents can promote leaching to some degree. Much debate surrounds the leaching mechanism, with oxidative addition of the aryl halide being common for organic solvents;[41] however, base and boronic acid promote leaching under aqueous conditions.[43]

The effect of the individual reagents on the morphology of the cubic catalysts, stirred separately in $EtOH/H_2O$ solutions of 4-methoxyiodobenzene, phenylboronic acid + K_2CO_3, K_2CO_3 and phenylboronic acid, was also assessed by TEM. After 24 h,

dx.doi.org/10.1021/cs5008014 | ACS Catal. 2014, 4, 3105−3111

the nanoparticles were collected and analyzed by TEM as shown in Figure 6. Stirring the aryl halide left the cubic

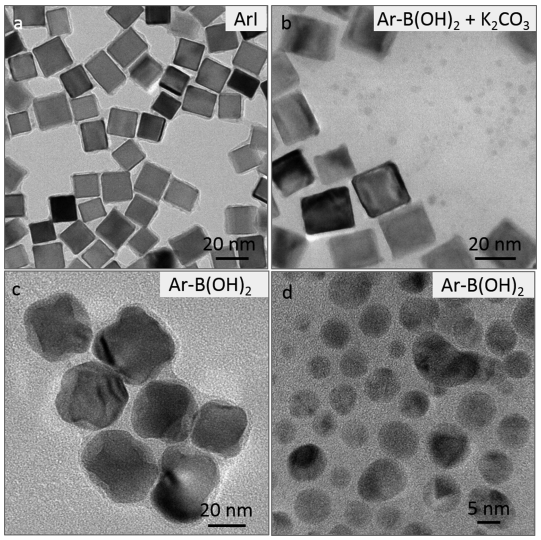

Figure 6. TEM images of cubic NCs after stirring in (a) MeO-Ph-I, (b) phenylboronic acid and K_2CO_3, (c) concave NCs, and (d) cubic NCs stirred in phenylboronic acid.

morphology excellently preserved (Figure 6a), and the presence of Pd clusters was not readily apparent. A mixture of boronic acid and base also left the cubic shape intact, but the presence of small diameter (1−2 nm) Pd nanoparticles was readily identified, similar to that observed in the post-reaction mixture. Finally, stirring the catalysts in the presence of the base alone caused no significant change in morphology, and no Pd clusters were observed by TEM (Supporting Information Figure S5). Interestingly, the boronic acid alone has the most significant influence on the morphology of the NCs; the concave cubic NCs lost their defined edges and became more spherical, as shown in Figure 6c. Many of the cubic NCs dissolved and the catalysts became spherical. The diameter of these particles was larger (5−10 nm) than those observed when the NCs are stirred in boronic acid + K_2CO_3. Unlike the base or aryl halide, the boronic acid can act as both a reducing agent for the leached Pd and a capping ligand that facilitates the formation of Pd nanoparticles.[50] Note that the overlayers surrounding the NCs in the TEM images arise from contamination during the reaction.

Filtration tests are commonly used to assess the homogeneity of heterogeneity of the reaction mechanism, although it has been noted that redisposition of the leached Pd make them unreliable.[51] Figure 7a shows the reaction profile catalyzed by concave cubes when the reaction mixture was filtered through activated carbon and washed with EtOH/H_2O, 90 min after the reaction was initiated. Comparison with the nonfiltrated reaction clearly show that formation of the biaryl product stops after filtration. This loss of catalytic activity can be attributed to the removal of both the parent NC and the Pd clusters formed due to leaching. TEM analysis of the activated carbon confirmed the capture of Pd clusters in addition to the concave cubes by filtration, as shown in Figure 7b,c. TEM analysis of the centrifuged filtrates did not contain Pd clusters which were present in the nonfiltered samples.

XPS analysis was used to determine if leaching gave rise to changes in the NC surface chemistry. Figure 8 shows the Pd 3d

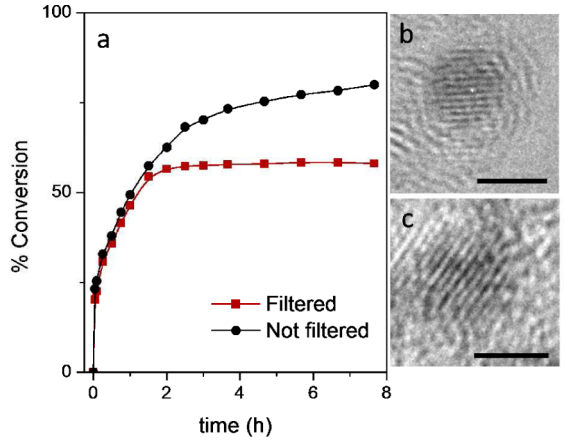

Figure 7. (a) Reaction profile of Suzuki coupling reactions catalyzed by concave Pd NCs showing the effect of filtration 90 min into the reaction. (b),(c) TEM image of Pd clusters captured on activated carbon after reaction filtration. Scale bar = 2 nm.

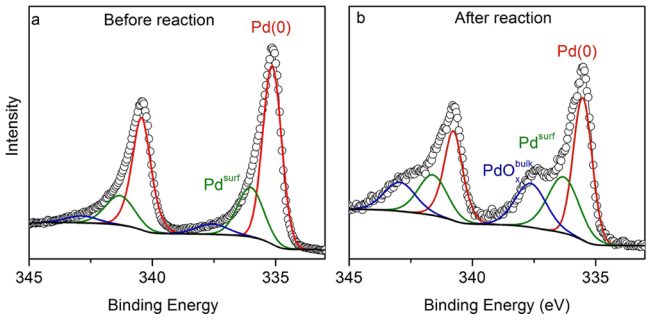

Figure 8. Pd 3d core level spectra of cubic NCs (a) before the reaction and (b) after the reaction. Spectrum (b) was collected using Pd catalysts from several reactions.

core level of the cubic NCs before and after the reaction. Before the reaction, the NCs primarily consisted of metallic Pd, as indicated by the Pd(0) peak at a binding energy of 335.0 eV. The small shoulder peak located at a binding energy of 336.1 eV is typically assigned to surface PdO and a very small peak at 337.1 eV assigned to bulk PdO_x.[46] Figure 8b shows the Pd spectrum after the reaction, with an increased intensity of the bulk PdO_x peak. The formation of oxide is consistent with the presence of Pd clusters, which undergo surface oxidation in the absence of stabilizing ligands. The survey spectra shows the presence of the N 1s peak at 400 eV, indicating retention of the PVP capping layer (Supporting Information Figure S6). A small reduction in the Pd/N ratio for the catalysts was observed after the reaction (i.e., Pd/N of 4 to 3.8 for the 10 nm cubic NCs and Pd/N of 2.7 to 2.3 for the concave cubic NCs). A more significant decrease in the Pd/Br ratio was observed, decreasing by 25% for the cubic NCs and 51% for the concave cubic NCs (Supporting Information Table S1).

The data obtained from the present study correlate well with the catalytic leaching mechanism, although the contribution of a heterogeneous mechanism cannot be completely ruled out. Although the parent NCs serve as reservoirs for more active Pd species, it is not possible to differentiate between the catalytic activity of solubilized Pd complexes and the Pd clusters observed by TEM. The significant difference in catalytic activity between the high- and low-index facet NCs suggests that leaching is the rate-determining step in this study. Atom

dx.doi.org/10.1021/cs5008014 | ACS Catal. 2014, 4, 3105−3111

abstraction energies for 3 nm spherical Pd nanoparticles were calculated to be 45 kcal mol^{-1}.[52] Atoms with lower coordination numbers, such as vertex and edge atoms, have lower abstraction energies compared to face atoms. Computational modeling of nanoparticle-catalyzed Suzuki coupling reactions are lacking; density functional theory (DFT) calculations based on homogeneous catalysts determined the typical activation energies for oxidative addition of aryl iodides and transmetalation to be 20−25 kcal mol^{-1}.[53,54] The relatively high activation energies for Pd leaching support the consensus that leaching is the rate-determining step. The surface atomic structure influences the stability and leaching susceptibility of Pd atoms and consequently catalytic activity. There are formally no step sites on {100} surfaces, whereas 42% of the atoms on a {730} surface are step sites, and therefore, the concave cubes have a high number of leachable atoms with lower abstraction energy compared to the cubic NCs. In the Suzuki reaction, the higher surface step atom density of the concave cubic catalysts facilitates more efficient leaching leading to the superior catalytic performance. The rapid leaching resulted in no measurable induction period for reactions involving concave cubic Pd NC catalysts. In contrast, a long lag time was observed with cubic NCs reflecting the slower leaching from close-packed surfaces.

CONCLUSIONS

Pd NCs with high-index surface facets display superior catalytic performance in Suzuki coupling reactions compared to low-index faces. The origin of enhanced catalytic activity associated with catalysts enclosed by high-index surfaces was investigated. Both cubic and concave cubic NCs show increasing TOFs with decreasing concentrations, often indicative of a leaching process. TEM analysis identified the presence of small diameter Pd clusters in solution after the reaction, indicating a homogeneous leaching mechanism. These Pd clusters were only observed after the formation of biphenyl (i.e., not observed during the induction period). The high number of surface atoms located at step sites on the concave cubic NCs make it more energetically favorable to leach atoms from high-index surface facets compared to close-packed surfaces on cubic NCs.

This work shows that understanding leaching processes is central to the design of heterogeneous catalysts for Suzuki coupling and similar reaction systems. The shape of catalyst NC can considerably influence the leaching properties and therefore catalytic activity of the NCs. Furthermore, the study illustrates relatively large NCs (>10 nm) serve as reservoirs for more active Pd species, which is consistent with previous reports. It is important to highlight that although homogeneous Pd generated through leaching is an important step in the catalytic cycle, it does not imply that the overall reaction mechanism is homogeneous. The exact nature of the active species remains unclear as the leached solubilized Pd is in equilibrium with the small diameter Pd clusters. If these clusters are active in the reaction, then further elucidation of this equilibrium and the use of smaller diameter Pd nanoparticles (<3 nm) has the potential to further optimize activity in Suzuki coupling reactions.

ASSOCIATED CONTENT

Supporting Information

TEM images of leached Pd nanoparticles in the reaction solution and the XPS survey spectra and quantification of concave and cubic catalysts after reaction can be found in the Supporting Information. This material is available free of charge via the Internet at http://pubs.acs.org/.

AUTHOR INFORMATION

Corresponding Authors

* (G.C.) E-mail: g.collins@ucc.ie. Fax: +353 (0)21 4205143. Tel.: +353 (0)21 4205143.
* (G.M.) E-mail: g.mcglacken@ucc.ie.

Notes

The authors declare no competing financial interest.

ACKNOWLEDGMENTS

We thank Enterprise Ireland (grant EI2011-0139) and Eli Lilly for supporting this research. We also acknowledge financial support from Science Foundation Ireland under award 08/CE/I1432.

REFERENCES

(1) Tian, N.; Zhou, Z.-Y.; Sun, S.-G.; Ding, Y.; Wang, Z. L. *Science* **2007**, *316*, 732−735.
(2) Quan, Z.; Wang, Y.; Fang, J. *Acc. Chem. Res.* **2013**, *46*, 191−202.
(3) Ford, L. P.; Nigg, H. L.; Blowers, P.; Masel, R. I. *J. Catal.* **1998**, *179*, 163−170.
(4) Liu, Z. P.; Hu, P. *J. Am. Chem. Soc.* **2003**, *125*, 1958−1967.
(5) Baker, T. A.; Xu, B.; Jensen, S. C.; Friend, C. M.; Kaxiras, E. *Catal. Sci. Technol.* **2011**, *1*, 1166−1174.
(6) Yin, L.; Liebscher, J. *Chem. Rev.* **2007**, *107*, 133−173.
(7) Antolini, E. *Energy Environ. Sci.* **2009**, *2*, 915−931.
(8) Torborg, C.; Beller, M. *Adv. Synth. Catal.* **2009**, *351*, 3027−3043.
(9) Collins, G.; O'Dwyer, C.; Morris, M.; Holmes, J. D. *Langmuir* **2013**, *29*, 11950−11958.
(10) Zhang, Q.; Russell, T. P.; Emrick, T. *Chem. Mater.* **2007**, *19*, 3712−3716.
(11) Xu, S.-Y.; Ruan, Y.-B.; Luo, X.-X.; Gao, Y.-F.; Zhao, J.-S.; Shen, J.-S.; Jiang, Y.-B. *Chem. Commun.* **2010**, *46*, 5864−5866.
(12) Lamblin, M.; Nassar-Hardy, L.; Hierso, J.-C.; Fouquet, E.; Felpin, F.-X. *Adv. Synth. Catal.* **2010**, *352*, 33−79.
(13) Choudary, B. M.; Madhi, S.; Chowdari, N. S.; Kantam, M. L.; Sreedhar, B. *J. Am. Chem. Soc.* **2002**, *124*, 14127−14136.
(14) Yuan, B.; Pan, Y.; Li, Y.; Yin, B.; Jiang, H. *Angew. Chem., Int. Ed.* **2010**, *49*, 4054−4058.
(15) Deraedt, C.; Astruc, D. *Acc. Chem. Res.* **2014**, *47*, 494−503.
(16) LeBlond, C. R.; Andrews, A. T.; Sun, Y. K.; Sowa, J. R. *Org. Lett.* **2001**, *3*, 1555−1557.
(17) Han, W.; Liu, C.; Jin, Z. *Adv. Synth. Catal.* **2008**, *350*, 501−508.
(18) Kim, S. W.; Kim, M.; Lee, W. Y.; Hyeon, T. *J. Am. Chem. Soc.* **2002**, *124*, 7642−7643.
(19) Lu, F.; Ruiz, J.; Astruc, D. *Tetrahedron Lett.* **2004**, *45*, 9443−9445.
(20) Collins, G.; Schmidt, M.; O'Dwyer, C.; Holmes, J. D.; McGlacken, G. P. *Angew. Chem., Int. Ed.* **2014**, *53*, 4142−4145.
(21) Crudden, C. M.; Sateesh, M.; Lewis, R. *J. Am. Chem. Soc.* **2005**, *127*, 10045−10050.
(22) Taladriz-Blanco, P.; Herves, P.; Perez-Juste, J. *Top. Catal.* **2013**, *56*, 1154−1170.
(23) Collins, G.; Blomker, M.; Osiak, M.; Holmes, J. D.; Bredol, M.; O'Dwyer, C. *Chem. Mater.* **2013**, *25*, 4312−4320.
(24) Hariprasad, E.; Radhakrishnan, T. P. *ACS Catal.* **2012**, *2*, 1179−1186.
(25) Mohanty, A.; Garg, N.; Jin, R. *Angew. Chem., Int. Ed.* **2010**, *49*, 4962−4966.
(26) Wang, F.; Li, C.; Sun, L.-D.; Wu, H.; Ming, T.; Wang, J.; Yu, J. C.; Yan, C.-H. *J. Am. Chem. Soc.* **2011**, *133*, 1106−1111.
(27) Jin, M.; Zhang, H.; Xie, Z.; Xia, Y. *Angew. Chem., Int. Ed.* **2011**, *50*, 7850−7854.

(28) Hong, J. W.; Kim, M.; Kim, Y.; Han, S. W. *Chem.—Eur. J.* **2012**, *18*, 16626−16630.
(29) Chen, Y.-H.; Hung, H.-H.; Huang, M. H. *J. Am. Chem. Soc.* **2009**, *131*, 9114−9121.
(30) Yu, Y.; Zhang, Q.; Liu, B.; Lee, J. Y. *J. Am. Chem. Soc.* **2010**, *132*, 18258−18265.
(31) Tian, N.; Zhou, Z.-Y.; Sun, S.-G. *Chem. Commun.* **2009**, 1502−1504.
(32) Chen, Y.-X.; Lavacchi, A.; Chen, S.-P.; di Benedetto, F.; Bevilacqua, M.; Bianchini, C.; Fornasiero, P.; Innocenti, M.; Marelli, M.; Oberhauser, W.; Sun, S.-G.; Vizza, F. *Angew. Chem., Int. Ed.* **2012**, *51*, 8500−8504.
(33) Tian, N.; Zhou, Z.-Y.; Yu, N.-F.; Wang, L.-Y.; Sun, S.-G. *J. Am. Chem. Soc.* **2010**, *132*, 7580−7581.
(34) Diaz Valenzuela, C.; Carriedo, G. A.; Valenzuela, M. L.; Zuniga, L.; O'Dwyer, C. *Sci. Rep.* **2013**, *3*, 2642.
(35) Le Bars, J.; Specht, U.; Bradley, J. S.; Blackmond, D. G. *Langmuir* **1999**, *15*, 7621−7625.
(36) Li, Y.; Hong, X. M.; Collard, D. M.; El-Sayed, M. A. *Org. Lett.* **2000**, *2*, 2385−2388.
(37) Davis, J. J.; Bagshaw, C. B.; Busuttil, K. L.; Hanyu, Y.; Coleman, K. S. *J. Am. Chem. Soc.* **2006**, *128*, 14135−14141.
(38) Davis, J. J.; Coleman, K. S.; Busuttil, K. L.; Bagshaw, C. B. *J. Am. Chem. Soc.* **2005**, *127*, 13082−13083.
(39) Ellis, P. J.; Fairlamb, I. J. S.; Hackett, S. F. J.; Wilson, K.; Lee, A. F. *Angew. Chem., Int. Ed.* **2010**, *49*, 1820−1824.
(40) Pachon, L. D.; Rothenberg, G. *Appl. Organometal. Chem.* **2008**, *22*, 288−299.
(41) Niu, Z.; Peng, Q.; Zhuang, Z.; He, W.; Li, Y. *Chem.—Eur. J.* **2012**, *18*, 9813−9817.
(42) Gaikwad, A. V.; Holuigue, A.; Thathagar, M. B.; ten Elshof, J. E.; Rothenberg, G. *Chem.—Eur. J.* **2007**, *13*, 6908−6913.
(43) Fang, P.-P.; Jutand, A.; Tian, Z.-Q.; Amatore, C. *Angew. Chem., Int. Ed.* **2011**, *50*, 12184−12188.
(44) Diallo, A. K.; Ornelas, C.; Salmon, L.; Aranzaes, J. R.; Astruc, D. *Angew. Chem., Int. Ed.* **2007**, *46*, 8644−8648.
(45) Thathagar, M. B.; ten Elshof, J. E.; Rothenberg, G. *Angew. Chem., Int. Ed.* **2006**, *45*, 2886−2890.
(46) Collins, G.; Schmidt, M.; McGlacken, G. P.; O'Dwyer, C.; Holmes, J. D. *J. Phys. Chem. C* **2014**, *118*, 6522−6530.
(47) Adrio, L. A.; Nguyen, B. N.; Guilera, G.; Livingston, A. G.; Hii, K. K. *Catal. Sci. Technol.* **2012**, *2*, 316−323.
(48) de Vries, A. H. M.; Mulders, J.; Mommers, J. H. M.; Henderickx, H. J. W.; de Vries, J. G. *Org. Lett.* **2003**, *5*, 3285−3288.
(49) Gaikwad, A. V.; Rothenberg, G. *Phys. Chem. Chem. Phys.* **2006**, *8*, 3669−3675.
(50) Narayanan, R.; El-Sayed, M. A. *J. Phys. Chem. B* **2005**, *109*, 4357−4360.
(51) Widegren, J. A.; Finke, R. G. *J. Mol. Catal. A* **2003**, *198*, 317−341.
(52) Ramezani-Dakhel, H.; Mirau, P. A.; Naik, R. R.; Knecht, M. R.; Heinz, H. *Phys. Chem. Chem. Phys.* **2013**, *15*, 5488−5492.
(53) Xue, L.; Lin, Z. *Chem. Soc. Rev.* **2010**, *39*, 1692−1705.
(54) Braga, A. A. C.; Ujaque, G.; Maseras, F. *Organometallics* **2006**, *25*, 3647−3658.